DTIP of MEMS & MOEMS Montreux, Switzerland, 12-14 May 2004

PERFORMANCE SIMULATION OF A MICROWAVE MICRO-ELECTROMECHANICAL SYSTEM SHUNT SWITCH USING CHATOYANT

Michael Bails[‡], Jose A. Martinez[‡], Steven P. Levitan[‡], Ilya Avdeev[╪], Michael Lovell[╪], Donald M. Chiarulli[†]

[‡]Department of Electrical Engineering, University of Pittsburgh
[╪]Department of Mechanical Engineering, University of Pittsburgh
[†]Department of Computer Science, University of Pittsburgh

ABSTRACT

The case study presented in this paper is a demonstration of our mixed-signal, multi-domain system level simulation tool Chatoyant. We have developed Chatoyant to support modeling and simulating of micro-opto-electro-mechanical systems. In this paper we demonstrate the capabilities of Chatoyant to model and simulate an RF MEMS shunt switch. We perform a system level simulation of the RF switch and verify our mechanical results using the commercial simulation packages, ANSYS and CoventorWare.

1. BACKGROUND

Chatoyant is a mixed signal, multi-domain CAD tool that can be used to design and analyze complete mixed-technology micro-systems [1]. Chatoyant is optimized for loosely coupled systems incorporating complex components, including electrical, optical, and mechanical devices that are now currently found in multi-domain microsystems.

Originally developed as an optical/electrical end to end system-level CAD tool [2] [3], Chatoyant has been expanded to MEMS and MOEMS modeling [4]. One such system of note was the simulation of the Grating Light Valve, which crossed the electrical, optical, and mechanical domains [1].

This paper focuses on the mechanical and electro-mechanical simulations of RF MEMS variable shunt capacitor switch.

2. CHATOYANT MECHANICAL MODELING

The mechanical domain of a component is modeled in Chatoyant as a set of differential equations that define the dynamic response of the device as it reacts to external forces. For the RF switch, these external forces come in the form of electro-static attraction between the moving plates and the substrate.

The mechanical elements are characterized by a template consisting of stiffness, mass, and damping matrices in a Modified Nodal Analysis (MNA) representation. The templates are developed by transforming the second order ordinary differential equation (ODE) of motion into a first order ODE for a piecewise linear (PWL) solution (Figure 1). The characteristic matrices, K (stiffness), B (damping), and M (mass), are static and independent of the dynamics in the body.

General motion equation

$$F = [K][U] + [B][\dot{U}] + [M][\ddot{U}]$$

Standard ODE Transformation

$$\begin{bmatrix} 0 & M \\ M & B \end{bmatrix} \begin{bmatrix} \ddot{U} \\ \dot{U} \end{bmatrix} + \begin{bmatrix} -M & 0 \\ 0 & K \end{bmatrix} \begin{bmatrix} \dot{U} \\ U \end{bmatrix} = \begin{bmatrix} 0 \\ I \end{bmatrix} F$$

Templates for every basic element (e.g. beam)

$$X = \begin{bmatrix} \dot{U} \\ U \end{bmatrix}; \quad [Mb]\dot{X} + [Mk]X = [E]F$$

Figure 1: Mechanical Matrix Representation

The two node beam elements are developed based on the Euler-Bernoulli beam equation [5]. Figure 2 shows a 2-D beam element stiffness matrix where L is the beam length, E is Young's Modulus, and I is the cross-sectional moment of inertia.

$$K = \frac{EI}{L^3} \begin{bmatrix} 12 & 6L & -12 & 6L \\ 6L & 4L^2 & -6L & 2L^2 \\ -12 & -6L & 12 & -6L \\ 6L & 2L^2 & -6L & 4L^2 \end{bmatrix}$$

Figure 2: 2-D Beam Stiffness Matrix

The development of the four node plate element is based on Kirchoff plate theory [6]. Here, the degrees of freedom (DOF) are separated into two components, in-plane displacements and bending (out-of-plane) displacements. The plate z-rotation (drilling DOF) is neglected for this analysis. This is accomplished by setting the diagonal entry of the stiffness matrix z-rotation to a suitably large number.

The equations for determining the stiffness and mass matrices for the remaining DOF (x, y, z, rotx, roty) are as follows:

$$\begin{aligned} u_x &= a_1 + a_2 x + a_3 xy + a_4 y \\ u_y &= a_5 + a_6 x + a_7 xy + a_8 y \end{aligned} \quad \text{In-plane} \qquad (1)$$

$$\begin{aligned} u_z &= a_1 + a_2 x + a_3 y + a_4 x^2 \\ &+ a_5 xy + a_6 y^2 + a_7 x^3 + a_8 x^2 y \\ &+ a_9 xy^2 + a_{10} y^3 + a_{11} x^3 y + a_{12} xy^3 \end{aligned} \quad \text{Bending} \qquad (2)$$

The (a) coefficients represent the DOF relating to the four node plate structure, and (x), (y) are coordinates of the nodes in the plane of the plate.

These matrices are developed based on the total DOF required for a given system. For example, if the plates are constrained to move only in x and y, equation (2) can be neglected. By controlling the degrees of freedom for the components in the system and using a PWL solver, a tradeoff between speed and accuracy can be realized.

3. RF MEMS DEVICE BACKGROUND

The RF MEMS device being investigated was developed and fabricated at the University of Michigan [7, 8] (Figure 3). The RF switch is similar to a parallel plate variable capacitor. The moving capacitive plate (C) is connected to actuation pads (A) which enable the structure to be displaced in the z-direction. The moving structure, composed of Nickel is suspended over a coplanar waveguide (CPW) and ground planes by a system of N-meander serpentine springs (B). Between the waveguide and the moving center capacitor is a 0.2μm insulating layer of silicon nitride ($\varepsilon_r = 7.5$). This is to prevent a short circuit from occurring in the signal path.

The number of meanders defining the spring system is integral to the switch speed and stability. For this paper, we considered a device having four meanders. The dimensions and material properties of the device are shown in Table 1.

This device works as an electro-mechanical shunt capacitor. When the switch is in the "off" mode, no applied voltage between ground and the actuation pads, very small attenuation of the RF signal is observed in the signal path. Applying a voltage to the actuation pads and thus setting the switch to the "on" position results in an increase in the coupling capacitance between the signal line and the center plate capacitor. This lowers the impedance between the signal and ground, thus effectively "shunting" the RF energy to ground and stopping the RF propagation through the signal line [9].

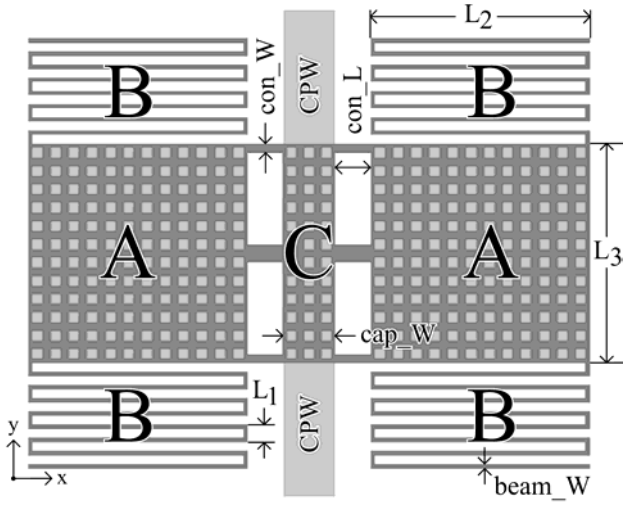

Figure 3: Schematic of RF Shunt Switch

Table 1: Geometry and Properties of the RF Switch

A	Actuation Pads (Ni)
C	Capacitor Pad (Ni)
CPW	Coplanar Waveguide
L1	20μm
L2, L3	250μm
cap_W	60μm
con_W	20μm
con_L	40μm
beam_W	5μm
Young's Modulus (Ni)	207GPa
Poisson's Ratio (Ni)	0.31
Density (Ni)	8909 kg/m^3
Gap	3μm
SiN_3 (above CPW)	0.2μm

4. RF MEMS SWITCH MODELING

In order to perform a system level simulation of the RF MEMS switch, it is necessary to investigate the mechanical and electro-mechanical properties of the switch. This includes determining the stiffness properties of the serpentine springs, modal analysis, pull-in voltage analysis of the system from the electrostatic actuation, and a circuit level model.

4.1. Serpentine Spring

The serpentine spring meanders, which suspend the switch above the substrate, play a major role in the switch speed and stability of the MEMS device. Our mechanical analysis for the serpentine spring is compared to the

mechanical simulations from ANSYS and CoventorWare [10].

4.1.1. Spring Stiffness Constant

The spring constant determines the stiffness of the serpentine meander structures. The importance of the stiffness to the MEMS designer is in the stability of the device. To evaluate the serpentine spring for the stiffness constant, a known force (1μN) is applied in the appropriate direction; the resulting displacement is used to determine the constant. In equation (3), the stiffness is equal to the applied force (F) divided by the displacement (x,y,z).

$$K = \frac{F}{(x, y, z)} \left[\frac{N}{m}\right] \tag{3}$$

Chatoyant performs a time-dependent dynamic analysis of the spring stiffness while ANSYS and CoventorWare Analyzer use static analyses. The Chatoyant time-dependency covers steady-state simulations and initial transients which are not available in static solvers.

The desired movement of the device is in the z-direction, however, there exists the possibility that x and y movement may occur, thus creating unwanted modulation of the RF signal. Table 2 displays the x, y, and z spring constants for the different solvers. The conditions for the analysis are found in Table 3.

Table 2: Four Meander Spring Stiffness Constant

	Stiffness (N/m)		
	Kz	Kx	Ky
Chatoyant	0.0543	1.749	0.372
ANSYS	0.0527	1.773	0.344
CoventorWare Architect	0.0546	1.863	0.396
CoventorWare Analyzer	0.0568	1.881	0.408

4.1.2. Modal Analysis – Spring Meander

The maximum frequency of operation for a four meander RF switch can be determined from the modal response. The modal results are important in that they ensure that any unwanted resonance, which may occur during circuit operation, is avoided.

Figure 4 shows the first nine modal frequencies in a four meander spring. Table 3 also gives the runtimes for the modal analysis for the different solvers. All analyses were performed on a P4 3.00 GHz processor with 2GB of SDRAM (disabling hyper-threading). Based on the results of Figure 4, there is good agreement between the different solvers.

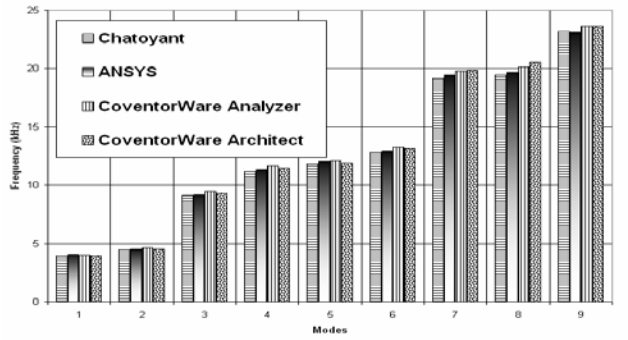

Figure 4: Modal Response of Spring Meander

4.1.3. Spring Dynamic Behavior

To dynamically test the spring meander system, a time-dependent force (1 μN) is applied in the z direction to the free end of the spring while anchoring the other end. Two switching speeds were investigated to see the dynamic ringing effects. The first dynamic response was based on a ramped input of 6ms (Figure 5). The displacement of the spring produces an almost linear response with this slow input rise time. The second dynamic response was based on a ramped input of 600μs (Figure 6). When the switching time is decreased by a factor of 10, the device is observed to show ringing oscillations. These oscillations could cause unwanted changes in the capacitance values during actuation. These results can guide the designer in setting the optimal switching speed in the device.

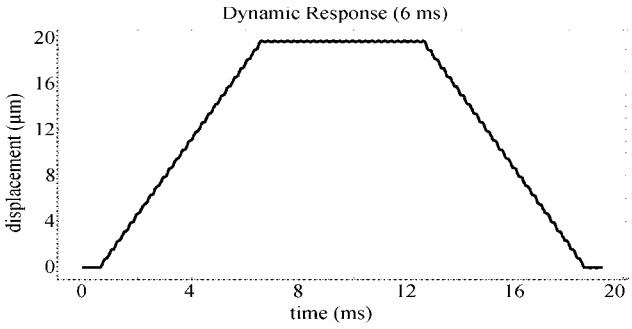

Figure 5: Switch Response - 6ms Rise Time

Table 3: Simulation Times for Modal Analysis

Simulation Time - Spring Modal Analysis		
Solver	**Simulation Time**	**Notes**
Chatoyant	1.107 seconds	Two Nodes per Element with Six Degrees of Freedom per Node
CoventorWare Architect	2.330 seconds	Nonlinear - One Segment Beam with Six Degrees of Freedom at Each Beam End
CoventorWare Analyzer FEM*	134.000 seconds	Manhattan Bricks - 27-Node Parabolic Elements (1664 Elements)
ANSYS FEM*	30.000 seconds	3-D 20-Node Structural Solid Element, Solid95 (1664 Elements)
*The FEM Element size is 2.5um x 2.5um x 2um		

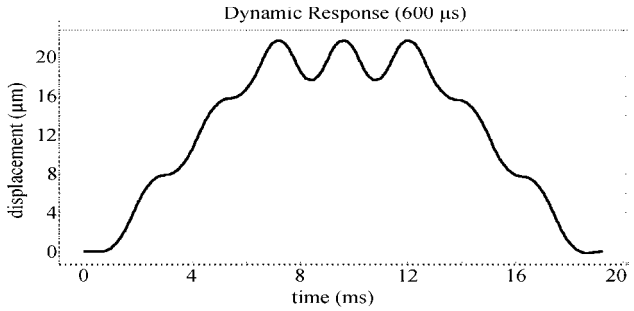

Figure 6: Switch Response - 600us Rise Time

4.2. Electrostatic Modeling

The electrostatic force between the actuation pads and the substrate determine the gap separation and the value of the shunt capacitor in the electrical circuit of the system. One of the primary considerations in the modeling of an electro-mechanical MEMS device is the pull-in voltage. Pull-in occurs when the electrical spring "softening," due to the nonlinear effects of the electrostatic applied force overcomes the mechanical stiffness of the device, thus snapping the device down to the substrate [10].

The Chatoyant electrostatic element is defined as an inclined flat capacitor. The distributed electrostatic forces are analytically represented as concentrated forces applied over each node in the element. The electrostatic force is given by:

$$F_i = \left(\frac{\varepsilon w V^2}{l}\right)\frac{(y_i - y_{i-1})^2}{\phi^2 y_i y_{i-1}} \qquad (4)$$

In the above equation, the φ represents the angle between the conductors, ε is the permittivity, V is the applied voltage, l is the length and w is the width of the element, y_i and y_{i-1} are the y coordinates of the nodes in the global reference frame.

Using a PWL linearization technique, the expression can be reduced to the form:

$$F_i = A_i V + A_i y_i + A_{i-1} y_{i-1} + A_0 \qquad (5)$$

The expression is a linear template that captures the nonlinear behavior of equation (4) through a set of coefficients (Ai, …A_0). This direct relationship between the electrical and mechanical domain necessitates the use of mixed domain solvers like Chatoyant.

The analytical equation for determining the pull-in voltage is given by:

$$V_{pi} = \sqrt{\frac{8K_z g_o^3}{27\varepsilon_o A}} \qquad (6)$$

In the above equation, K_z is the total mechanical spring stiffness for the structure (equal to $4*k_z$, where k_z is the individual spring constant of each serpentine spring in the system), g_o is the initial gap between the actuation pads and ground, ε_o is the free-space permittivity, and A is the area of the actuators.

4.2.1. Pull-in Analysis in Chatoyant

Chatoyant performs a co-simulation of the mechanical and electrical domains using the PWL solver to evaluate the pull-in voltage. The actuator drive voltage is applied dynamically to the nodal coordinates on the pads. The boundary conditions are such that the total displacement is equal to the gap. Figure 7 shows the Chatoyant simulation of pull-in voltage.

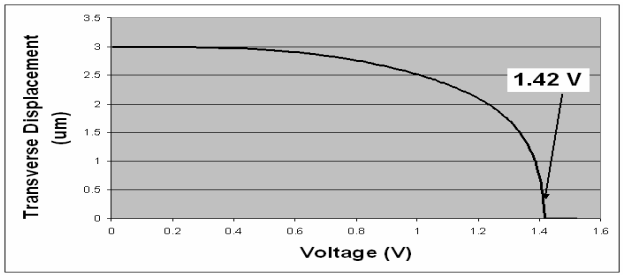

Figure 7: Chatoyant Pull-in Voltage Analysis

4.2.2. Pull-in Analysis in ANSYS

Using the CMATRIX macro from ANSYS, the value of capacitance vs. gap including fringing fields and holes

can be determined. Figure 8 shows a 3-D cross-section of the suspended capacitor surrounded by air. The plate is assumed to be a perfect conductor which allows the user to model only the exterior nodes of the plate. Closer inspection reveals the air holes in the plate are also modeled. The plate and ground are defined as conductors and the air is modeled using 3-D 20-node electrostatic solid elements. The nodal solution presented in the figure displays the magnitude of the electric field including fringing fields between the two conductors.

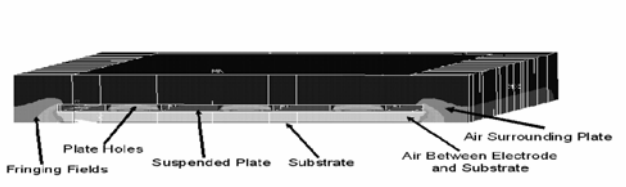

Figure 8: ANSYS Capacitance Extraction

Using ANSYS, the capacitance versus displacement (or stroke) function is developed by slightly decreasing the value of the gap and re-enabling the CMATRIX command. Figure 9 displays the nonlinearity effects of the shrinking gap.

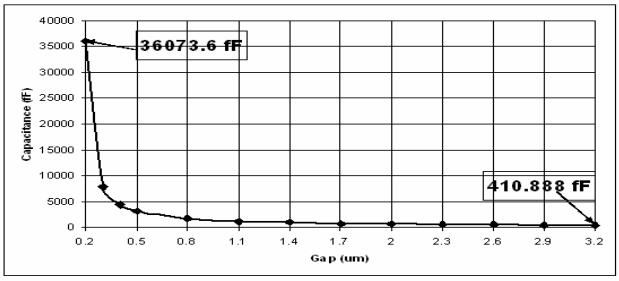

Figure 9: ANSYS Capacitance vs Stroke

These capacitance values can be placed in a lumped model in ANSYS for pull-in voltage analysis. Using the element TRANS126 (electro-mechanical transducer element), the finite element pull-in voltage of the RF switch can be determined. This is accomplished by applying a voltage sweep to the lumped model and determining the output. The approximate pull-in voltage for the RF switch with four meanders including holes is 1.36 V (Figure 10). This is compared to the analytical value from equation 5 based on the four meander system of 1.50 V and Chatoyant of 1.42 V. The differences in pull-in values can be attributed to the inclusion of fringing fields in ANSYS which increases overall capacitance, thus lowering the pull-in voltage.

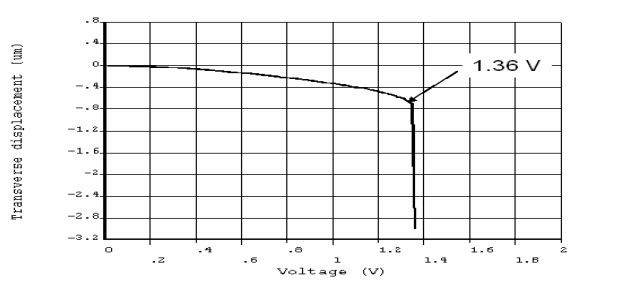

Figure 10: ANSYS Pull-in Analysis

4.3. Circuit Simulation

The circuit level model of the RF shunt switch system is composed of a 40 GHz RF having an AC amplitude of 5 V with a source impedance of 50Ω. A load resistor of 50Ω is included in parallel with the variable capacitor. The variable capacitor represents the mechanical RF switch (Figure 11).

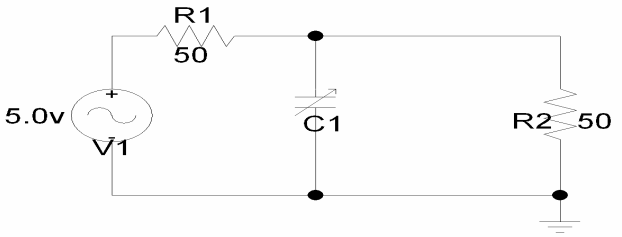

Figure 11: Circuit Schematic of RF MEMS System

ANSYS CMATRIX macro was again used to determine the capacitance vs. stroke for the center capacitor. These values were used in SPICE [11] as sweep variables to in order to see the effects of the switch on the magnitude of the output voltage. Not only does the signal experience a phase shift (due to the input impedance), but as the gap decreases, the magnitude of the output signal experiences a -23.7 dB loss. Figure 12 displays snapshots of the output signal under differing values of capacitance.

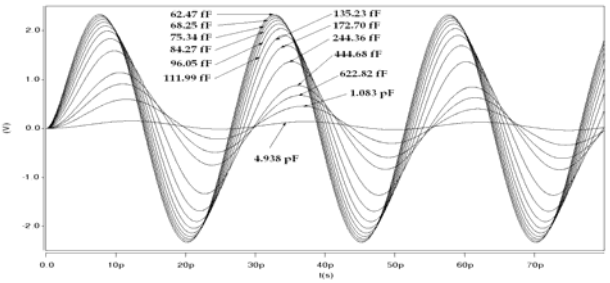

Figure 12: Switch Analysis with Variable Capacitance

4.4. End to End Simulation

Combining the electrical and mechanical domains into a co-simulation environment, Chatoyant can perform a dynamic end to end full system analysis. The schematic of the simulation is shown in Figure 13. A sine-function generator (singen) is used to produce the 40GHz signal and a piecewise linear input is used to drive the RF switch. The transmission lines (TL) include source and load impedances.

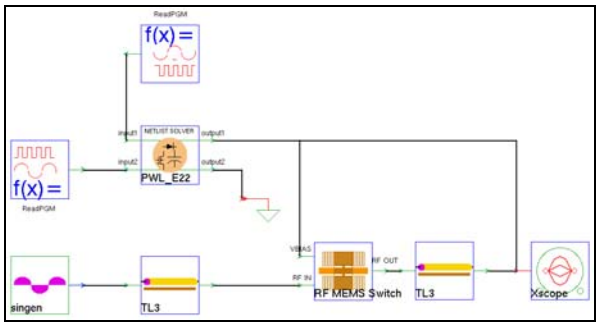

Figure 13: Chatoyant Schematic of Full System

This integrated system allows us to not only perform a pull-in analysis above, but in the same simulation, using the output from the center capacitance, we can perform a full system simulation. This transient analysis uses the electrical input of the 40GHz input taking the output from the switch (Figure 14).

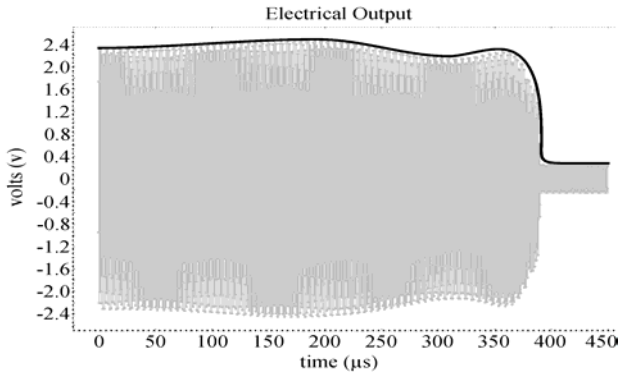

Figure 14: Transient Response of RF MEMS Switch

From the figure, we can see the operation of the switch and the response of the electrical signal. The magnitude of the signal envelope is greatly attenuated due to the switch actuation.

5. SUMMARY AND CONCLUSION

This ongoing analysis of the RF MEMS shunt switch capacitor provides a good test for Chatoyant's capabilities to model mixed-domain systems. The mechanical complexities of the spring (beam model) assembly along with the actuation and capacitance pads (plate model) are coupled with the electro-mechanical forces, thus creating the variable capacitor.

The stiffness, modal response, dynamic switching, and pull-in voltage are integral to modeling of this and other MEMS devices. While each of these analysis can be done separately using commercial tools, complete system level simulation gives more insight to the designer, and provides a single environment for design trade-offs.

Some considerations not covered in this paper for future analysis are to incorporate residual stresses of the device. This includes curvature from fabrication stresses and possible design errors. Another consideration for future work is to develop a damping model for Chatoyant to include coquette and squeezed-film damping.

6. REFERENCES

[1] S.P. Levitan, et al, "System Simulation of Mixed-Signal Multi-Domain Microsystems With Piecewise Linear Models." IEEE Trans. On CAD. Vol. 22 n. 2, Feb. 2003, pp. 139-154.

[2] S.P. Levitan, et al, "Chatoyant, a Computer-Aided Design Tool for Free-Space Optoelectronic Systems, "Applied Optics, Vol. 37, No. 26, pp. 6078-6093, (10 Sept. 1998).

[3] Mark Kahrs, et al, "System-level Modeling and Simulation of the 10G Optoelectronic Interconnect," IEEE Journal of Selected Topics in Quantum Electronics.

[4] T.P. Kurzweg, et al, "Modeling Optical MEM Systems," Journal of Modeling and Simulation of Microsystems (JMSM), Vol. 2, No. 1, 2001, pp. 21-34.

[5] Przemieniecki, J.S. Theory of Matrix Structural Analysis, Dover Publications, Inc. New York, 1985.

[6] ANSYS Multiphysics/LS-DYNA Release 7.0, ANSYS Inc., Cannonsburg, PA. www.ansys.com.

[7] S.P. Pacheco, et al, "Design of low actuation voltage RF MEMS switch," in IEEE MTT-S Int. Microwave Symp. Dig., vol 1, June 2000, pp. 165-168.

[8] Peroulis, D., et al, "Electromechanical Considerations in Developing Low-Voltage RF MEMS Switches," in IEEE Trans. On Micro. Theory and Techniques, vol 51, no. 1, Jan 2003, pp. 259-270.

[9] Yao, J. Jason, "RF MEMS from a device perspective," in J. Micromech. Microeng., vol. 10, 2000, pp. R9-R38.

[10] CoventorWare version2003.1, Coventor, Inc., Cary, NC. www.coventor.com.

[11] Senturia, Stephen D. Microsystem Design, Kluwer Academic Publishers, Boston, 2001.

[12] HSPICE version: U-2003.09-SP1, www.synopsys.com.